Article

Cell Reports

Endothelial Sash1 Is Required for Lung Maturation through Nitric Oxide Signaling

Graphical Abstract

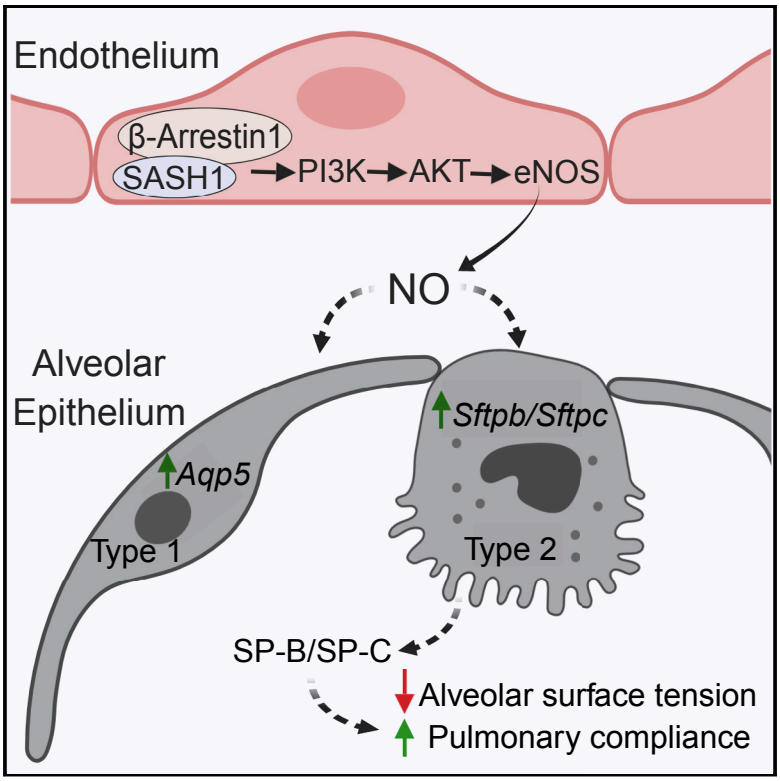

Authors

Patrick Coulombe, Grigorios N. Paliouras, Ashley Clayton, ..., Jeremy D.K. Parker, Joanne L. Wright, Aly Karsan

Correspondence

akarsan@bcgsc.ca

In Brief

Surfactant deficiency due to lung immaturity is a major cause of respiratory distress in premature newborns. Coulombe et al. show that endothelial SAM and SH3 domain containing protein 1 (Sash1) drives perinatal lung maturation via nitric oxide signaling to alveolar cells. Sash1 interacts with β-arrestin1 to activate Akt-eNOS and induce alveolar epithelial cell maturation and surfactant synthesis.

Highlights

- Sash1 signaling in the pulmonary endothelium triggers alveolar cell maturation
- Sash1 interacts with β-arrestin1 to activate Akt-eNOS
- Endothelial NO stimulates alveolar cell maturation in an sGC-cGMP-dependent manner

Coulombe et al., 2019, Cell Reports 27, 1769–1780
May 7, 2019
https://doi.org/10.1016/j.celrep.2019.04.039

CellPress

Cell Reports
Article

Endothelial Sash1 Is Required for Lung Maturation through Nitric Oxide Signaling

Patrick Coulombe,[1,2] Grigorios N. Paliouras,[1] Ashley Clayton,[1,2] Angela Hussainkhel,[1,3] Megan Fuller,[1] Vida Jovanovic,[1] Shauna Dauphinee,[1,2] Patricia Umlandt,[1] Ping Xiang,[5] Alistair H. Kyle,[6] Andrew I. Minchinton,[6] R. Keith Humphries,[4,5] Pamela A. Hoodless,[4,5] Jeremy D.K. Parker,[1] Joanne L. Wright,[7] and Aly Karsan[1,2,3,7,8,*]

[1]Michael Smith Genome Sciences Centre, BC Cancer Agency, 675 West 10th Avenue, Vancouver, BC V5Z 1L3, Canada
[2]Department of Experimental Medicine, University of British Columbia, Vancouver, BC V6T 2B5, Canada
[3]Program of Interdisciplinary Oncology, University of British Columbia, Vancouver, BC V6T 2B5, Canada
[4]Department of Medical Genetics, University of British Columbia, Vancouver, BC V6T 2B5, Canada
[5]Terry Fox Laboratory, BC Cancer Agency, 675 West 10th Avenue, Vancouver, BC V5Z 1L3, Canada
[6]Department of Integrative Oncology, BC Cancer Research Centre, 675 West 10th Avenue, Vancouver, BC V5Z 1L3, Canada
[7]Department of Pathology, University of British Colombia, Vancouver, BC V6T 2B5, Canada
[8]Lead Contact
*Correspondence: akarsan@bcgsc.ca
https://doi.org/10.1016/j.celrep.2019.04.039

SUMMARY

The sterile alpha motif (SAM) and SRC homology 3 (SH3) domain containing protein 1 (Sash1) acts as a scaffold in TLR4 signaling. We generated *Sash1*$^{-/-}$ mice, which die in the perinatal period due to respiratory distress. Constitutive or endothelial-restricted *Sash1* loss leads to a delay in maturation of alveolar epithelial cells causing reduced surfactant-associated protein synthesis. We show that Sash1 interacts with β-arrestin 1 downstream of the TLR4 pathway to activate Akt and endothelial nitric oxide synthase (eNOS) in microvascular endothelial cells. Generation of nitric oxide downstream of Sash1 in endothelial cells affects alveolar epithelial cells in a cGMP-dependent manner, inducing maturation of alveolar type 1 and 2 cells. Thus, we identify a critical cell nonautonomous function for *Sash1* in embryonic development in which endothelial Sash1 regulates alveolar epithelial cell maturation and promotes pulmonary surfactant production through nitric oxide signaling. Lung immaturity is a major cause of respiratory distress and mortality in preterm infants, and these findings identify the endothelium as a potential target for therapy.

INTRODUCTION

The alveolar unit of the lung forms a complex structure, with extensive surface area, closely associated with blood vessels to maximize gas exchange at the alveolar-capillary interface (Hsia et al., 2016). Primitive alveoli are formed from epithelial-lined saccules during the saccular stage of lung development (Hsia et al., 2016). Initiated at embryonic day 17.5 (E17.5) in mice, this process extends to postnatal day 5 (P5), when the final stage of alveolar maturation begins to increase surface area and promote better gas exchange (Warburton et al., 2010; Woik and Kroll, 2015). Initiation of surfactant production before birth is essential to permitting ventilation and premature birth is often associated with respiratory distress due to surfactant deficiency (Woik and Kroll, 2015).

Pulmonary surfactant is a rich complex of phospholipids, mainly phosphatidylcholine and phosphatidylglycerol, that are associated with specific surfactant proteins and cholesterol (Dobbs, 1989; Perez-Gil and Weaver, 2010). The lipid-protein interaction of surfactant is responsible for reducing surface tension at the air-tissue interface within the alveoli, which facilitates lung inflation (Weaver and Conkright, 2001; Perez-Gil and Weaver, 2010). The alveolar wall comprises mainly alveolar epithelial type 1 (AE1) cells that form the air-blood barrier along with the capillary endothelium, whereas less abundant alveolar epithelial type 2 (AE2) cells are responsible for the synthesis, secretion, and recycling of surfactant components (Hsia et al., 2016; Dobbs and Johnson, 2007). The protein and lipid surfactant components are secreted separately and assembled into the lamellar bodies of AE2 cells, associated with a decrease in cytoplasmic glycogen (Rooney et al., 1994; Perez-Gil and Weaver, 2010; Young et al., 1991). Four types of surfactant-associated proteins (SPs) are independently secreted from AE2 cells. SP-B and SP-C reduce surface tension, and their secretion is respectively limited to AE2 and Clara cells or AE2 cells only (Cochrane and Revak, 1991; Weaver and Conkright, 2001). In contrast, SP-A and SP-D are more widely expressed and have been described to be involved in innate immune signaling (Carreto-Binaghi et al., 2016).

Administration of antenatal glucocorticoids is an important part of patient management of pregnancies at risk of preterm birth to promote the maturation of the fetal lung (Schellhase and Shannon, 1991; Jobe and Goldenberg, 2018). In addition to corticosteroids, intrauterine inflammation affects the developing lung potentially through an independent pathway (Moss

and Westover, 2017). Chorioamnionitis is a major cause of preterm births and is associated with reduced risk of respiratory distress syndrome (Watterberg et al., 1996; Moss and Westover, 2017). Infection-driven models of chorioamnionitis suggested that induced inflammation, triggered by interleukin 1 (IL-1) or lipopolysaccharide (LPS) overexpression, can accelerate lung development, shown by increased SP-A expression (Willet et al., 2002; Hillman et al., 2008), but the mechanism is poorly understood (Moss and Westover, 2017). However, models of chorioamnionitis do not reflect the normal progression of lung development in healthy individuals. Hence, much remains to be learned about the pathways regulating prenatal lung alveolar maturation.

Toll-like receptors (TLRs) are key mediators of the innate immune system. The TLR4 response to LPS stimulation triggers the release of proinflammatory cytokines through a MyD88-dependent signaling cascade involving the recruitment of the TNF receptor associated factor-6 (TRAF6) that culminates in activation of MAPK and NF-κB pathways (Lu et al., 2008; Dauphinee and Karsan, 2006). Additionally, we have shown that LPS stimulation activates the phosphatidylinositol 3′ kinase (PI3K)-Akt pathway in endothelial cells independently of TRAF6 (Dauphinee et al., 2011). More recently, we identified SASH1 (sterile alpha motif [SAM] and SRC homology 3 [SH3] domain containing protein 1) as a scaffold molecule downstream of TLR4 that binds TRAF6 to facilitate NF-κB activation (Dauphinee et al., 2013).

Initially described as a tumor suppressor, SASH1 is a large multidomain protein encoded by 20 exons and belonging to the SLY family of adaptor proteins (Zeller et al., 2003). Sash1 is strongly expressed in microvascular endothelial cells but not in epithelial cells of the mouse lung (Dauphinee et al., 2013). Here, we show that homozygous disruption of *Sash1* in endothelial cells leads to delayed lung maturation, loss of surfactant production, and perinatal lethality. Sash1 interacts with β-arrestin and mediates phosphorylation and activation of Akt and endothelial nitric oxide synthase (eNOS) downstream of TLR4 in pulmonary endothelial cells. Endothelial-generated nitric oxide (NO) activates soluble guanylyl cyclase (sGC) in alveolar epithelial cells to promote lung parenchymal maturation and induce surfactant-associated genes. In *Sash1*$^{-/-}$ mice, surfactant production and AE1 maturation is restored either by an NO donor or sGC activator. Our findings demonstrate a critical role for innate immune signaling in generating NO in the pulmonary microvascular endothelium during development to promote lung maturation and stimulate surfactant protein production.

RESULTS

Sash1$^{-/-}$ Mice Die Perinatally

To study the *in vivo* function of Sash1, we generated a transgenic mouse model using ESCIs in which a gene-trap vector was inserted into intron 14 of the *Sash1* allele (Dauphinee et al., 2013). Genetic disruption of *Sash1* generated a Sash1-LacZ fusion protein composed of the first 14 exons of *Sash1*, followed by the β-geo construct under the control of the endogenous *Sash1* promoter (Figure S1). The Sash1-LacZ fusion protein lacks the SH3 domain, both SAM domains, and the TRAF6-binding domain (Dauphinee et al., 2013). Mice homozygous for the *Sash1* gene-trap (*Sash1*$^{-/-}$) died perinatally and were slightly smaller than their heterozygous and wild-type (WT) littermates (Figure 1A). Matings between heterozygous mice produced offspring with a Mendelian distribution of WT, heterozygotes (*Sash1*$^{+/-}$), and homozygotes (*Sash1*$^{-/-}$) (Figure 1B). At birth, WT and heterozygous pups were pink with a regular breathing pattern and active limb movements. In contrast, *Sash1*$^{-/-}$ pups were cyanotic and died immediately postnatally, secondary to respiratory distress, even though animals appear to be moving when born at term (P0) (Figure 1A). Visually, no gross anatomical differences during embryonic development were observed when comparing WT and *Sash1*$^{-/-}$ mice at E17.5 (Figure S2). Despite respiratory distress at birth, examination of *Sash1*$^{-/-}$ lungs during development revealed no significant difference between *Sash1*$^{-/-}$ and WT lung weights relative to body weight. A significant difference in the body weight of *Sash1*$^{-/-}$ mice was not observed until E17.5 compared to littermate controls (Figure S2). These data show that *Sash1*$^{-/-}$ mice developed normally until late gestational age and that Sash1 may be important in late-stage fetal lung development.

Visual inspection of *Sash1*$^{-/-}$ mice at birth led to the hypothesis that newborn *Sash1*$^{-/-}$ mice died due to an inability to take their first breath. A lung buoyancy test (Große Ostendorf et al., 2013) was performed with lungs isolated from WT and *Sash1*$^{-/-}$ mice at E18.5 and P0 (Figure 1C). While WT lungs were inflated and floated when placed in PBS, *Sash1*$^{-/-}$ lungs did not float and sunk to the bottom (Figure 1C), supporting the hypothesis that *Sash1*$^{-/-}$ lungs did not inflate after birth. Further histological analysis of H&E-stained lung tissue confirmed the conclusion that the alveoli of the *Sash1*$^{-/-}$ mice were collapsed (Figure 1D). Artificial inflation of *Sash1*$^{-/-}$ lungs using 0.75% agarose instillation through the trachea revealed alveolar structures and no obvious morphological differences in lung structure (Figure 1E).

Surfactant Protein Production Is Defective in Lungs of *Sash1*$^{-/-}$ Embryos

The pulmonary surfactant complex of phospholipids and surfactant proteins secreted by mature alveolar epithelial type 2 (AE2) cells functions to maintain a low alveolar surface tension and thereby prevent atelectasis. Immature AE2 cells contain an abundant amount of cytoplasmic glycogen as a substrate for the synthesis of surfactant (Bourbon et al., 1982; Young et al., 1991), and maturation of AE2 cells is concomitant with a marked decrease in glycogen content and a simultaneous increase in the number of lamellar bodies that store pulmonary surfactant (Young et al., 1991). To assess intracellular glycogen in pulmonary epithelial cells, periodic acid Schiff (PAS) staining was performed on E18.5 lung sections. In comparison to WT embryos, there was a significantly greater number of epithelial cells in *Sash1*$^{-/-}$ embryonic lungs that were positive for PAS staining (Figure 2A), suggesting glycogen accumulation. Transmission electron microscopy (TEM) of *Sash1*$^{-/-}$ lungs confirmed that the cytoplasm of AE2 cells contained more glycogen than WT lungs (Figure 2B), suggesting that AE2 cells of *Sash1*$^{-/-}$ animals had not assembled surfactant complexes. Importantly, no morphological or ultrastructural defects of the lung architecture were observed (Figures 2B and S3A).

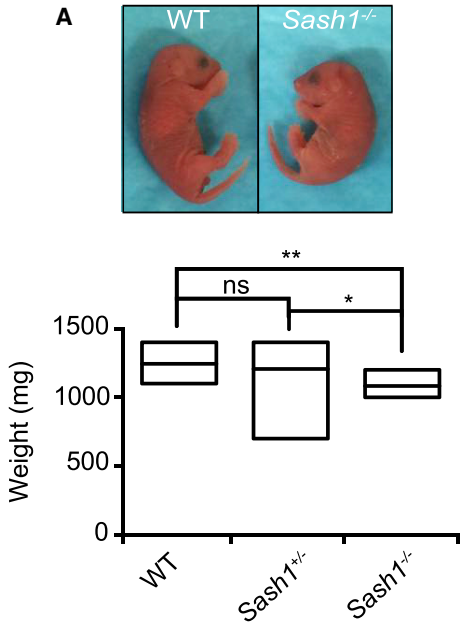

B

Genotype	Observed Born	Expected Born	
WT	18	17.75	χ^2 = 1.141
Sash1$^{+/-}$	39	35.5	p-value = 0.565
Sash1$^{-/-}$	14	17.75	Mendelian
Total	71		

Genotype	Observed live pups after birth	Expected live pups at birth	
WT	18	14.25	χ^2 = 19.105
Sash1$^{+/-}$	39	28.5	p-value = 0.0001
Sash1$^{-/-}$	0	14.25	non-Mendelian
Total	57		

E18.5	Float	Sink
WT + *Sash1*$^{+/-}$	26	0
Sash1$^{-/-}$	0	7 (p = 0.0001)

P0	Float	Sink
WT + *Sash1*$^{+/-}$	21	1
Sash1$^{-/-}$	0	7 (p = 0.0001)

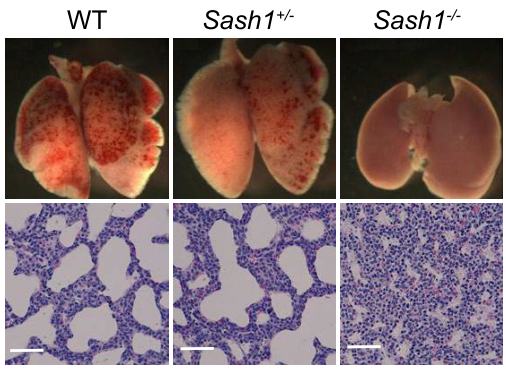

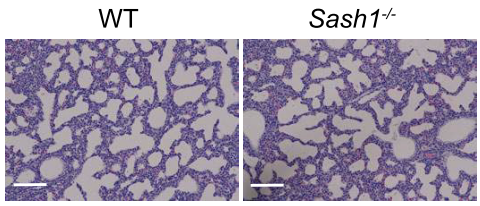

Figure 1. Characterization of the Lung Defect in *Sash1*$^{-/-}$ Neonates

(A) Representative images of pups at birth and weight of mice at birth based on their genotype (n = 9 WT, 14 *Sash1*$^{+/-}$, and 6 *Sash1*$^{-/-}$).

(B) Total number of pups born (upper panel) and those alive at birth (lower panel) for each genotype, compared to the expected Mendelian ratio.

(C) Image of a buoyancy test performed in PBS with lungs at birth. Lungs were enumerated based on whether they floated or sank at E18.5 and P0.

(D and E) H&E staining of lung sections at birth before (D) and after (E) inflation with 0.75% agarose (scale bars: 50 μm in D and 25 μm in E) (*p < 0.05, **p < 0.01). See also Figures S1 and S2.

A lack of surfactant could explain the inability of *Sash1*$^{-/-}$ mice to inflate their lungs at birth. We thus directly assessed the ability of *Sash1*$^{-/-}$ pulmonary epithelial cells to synthesize the four surfactant-associated proteins in the lung: SP-A, SP-B, SP-C, and SP-D (Kuroki and Voelker, 1994). Overall expression levels of surfactant transcripts were significantly lower in *Sash1*$^{-/-}$ mice

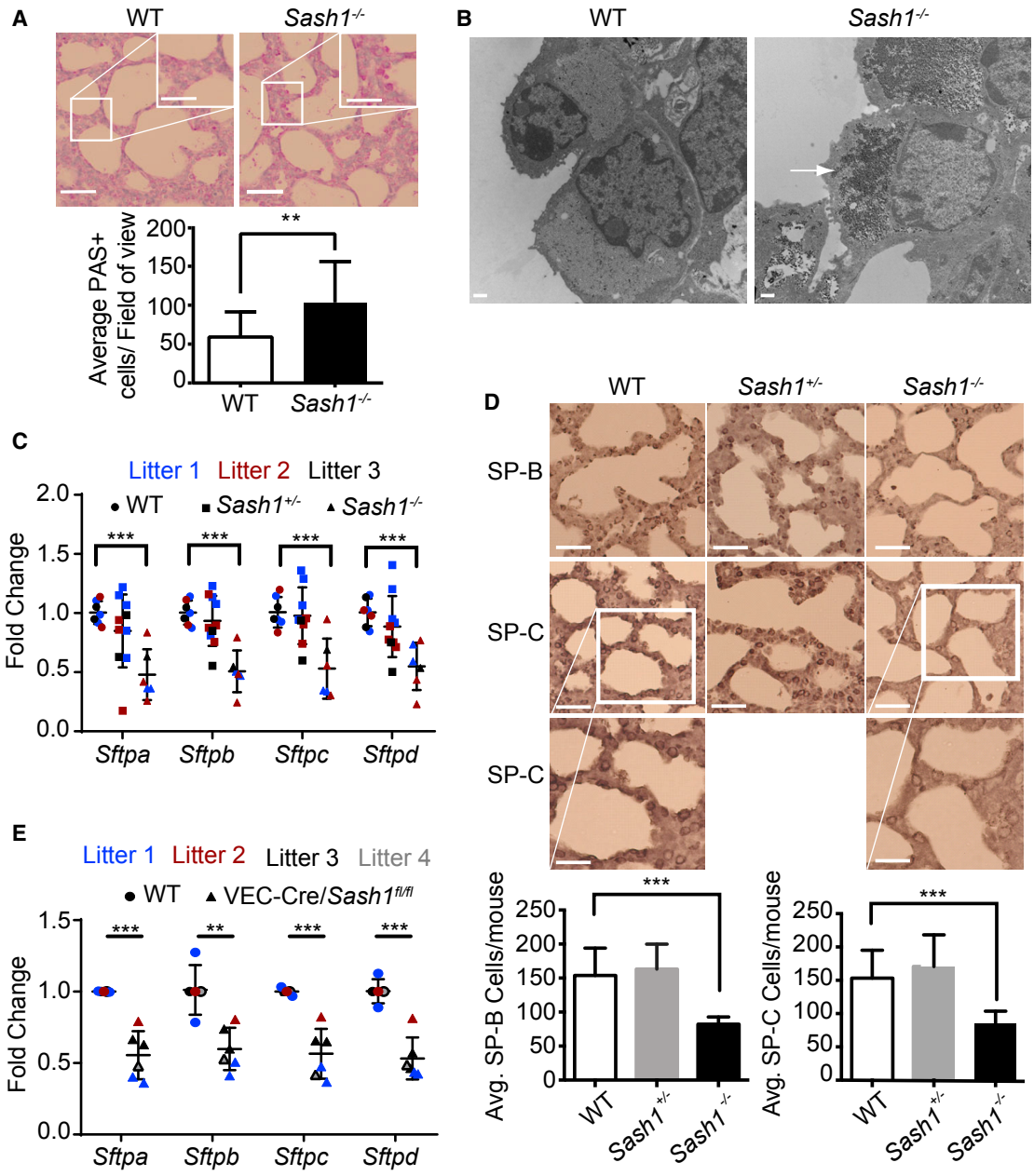

Figure 2. *Sash1*$^{-/-}$ Mice Have Reduced Surfactant Production at Birth

(A) Periodic acid Schiff (PAS) staining of E18.5 lung sections (scale bars: 50 and 25 μm; inset). Positive cells were counted per field of view and data reported as mean ± SD (n = 18 WT and 20 *Sash1*$^{-/-}$).

(B) Transmission electron microscopy showing increased glycogen content (arrow points to circular electron-dense granules, right panel) in lungs of E18.5 *Sash1*$^{-/-}$ embryos (scale bar, 500 nm).

(C) Expression of mRNA transcripts of surfactant-associated proteins by qRT-PCR using total RNA extracted from E18.5 lungs. Data normalized to *Gapdh* represented as fold-change compared to WT littermate, shown as mean ± SD (n = 7 WT, 10 *Sash1*$^{+/-}$, and 6 *Sash1*$^{-/-}$).

(D) Total number of SP-B and SP-C positive cells were quantified following immunohistochemical staining of WT, *Sash1*$^{+/-}$, and *Sash1*$^{-/-}$ P0 lungs (scale bar, 50 μm). (Lower panels) Enlargements of the indicated regions above for SP-C (scale bar, 25 μm). Six random fields of view were counted per mouse lung and the average number of SP-B and SP-C positive cells per mouse was plotted as mean ± SD for each genotype (n = 8 WT, 11 *Sash1*$^{+/-}$, and 6 *Sash1*$^{-/-}$).

(E) Expression of surfactant mRNA transcripts, by qRT-PCR, in E18.5 lungs. Data normalized to *Gapdh* represented as fold-change compared to WT littermate, shown as mean ± SD (n = 5 WT and 6 VEC-Cre-*Sash1*$^{fl/fl}$) (*p < 0.05, **p < 0.01, ***p < 0.001).

Each symbol color in (C) and (E) represents mice derived from the same litter.

compared to WT littermate controls, with variable levels present in the heterozygotes (Figure 2C). Immunohistochemical (IHC) staining of the surfactant proteins responsible for reducing surface tension at the air-fluid interface (SP-B and SP-C) were consistent with the mRNA data, as *Sash1*$^{-/-}$ mice showed reduced expression of these proteins in AE2 cells (Figure 2D). Thus, the marked surfactant-associated protein deficiency together with the abnormal accumulation of intracellular glycogen in the pulmonary epithelial cells suggests incomplete AE2 cell maturation and reduced synthesis and secretion of surfactant in Sash1$^{-/-}$ embryonic lungs.

Sash1-Dependent Endothelial Function Is Required for Lung Maturation

Sash1 mRNA expression has been found to be highly elevated in the microvasculature of several organs, with expression levels found to be highest in the lung, spleen, thymus, and placenta (Dauphinee et al., 2013). Specifically, we have reported that *Sash1* is selectively expressed in microvascular endothelial, but not epithelial, cells of the adult mouse lung (Dauphinee et al., 2013). The genetic and cellular programs that regulate the timing of lung maturation are tightly controlled, and endothelial growth factors have been suggested to play a role in fetal lung maturation (Xu et al., 2012; Ding et al., 2011). As in the adult, Sash1 expression was restricted to endothelial cells in the embryonic lung (Figure S3B). No difference was seen in the vascular density or endothelial cell distribution of *Sash1*$^{-/-}$ embryonic lungs by CD31 staining (Figures S3C–S3E). TEM showed a similar juxtaposition of endothelial cells with AE2 cells and perfusion of the microvasculature at E18.5 (Figure S3A). Additionally, flow cytometry analysis revealed no differences in the total number of CD31^{+} endothelial cells, the AE2-enriched EpCAM^{+}T1α^{lo} population, or the AE1-enriched EpCAM^{+}T1α^{hi} population. (Figure S4). The ratios between these various cell populations were also unaffected (Figure S4). These findings suggest that structural abnormalities of the alveolar endothelial-epithelial unit are not responsible for the phenotype observed in *Sash1*$^{-/-}$ mice, and that the surfactant defect stems from endothelial Sash1 functional activity.

To confirm that the phenotype observed in *Sash1*$^{-/-}$ mice originated from the endothelium, we generated a conditional *Sash1*-floxed mouse (*Sash1*$^{fl/fl}$) by flanking exons 3 and 4 of the *Sash1* gene with LoxP sites. We deleted *Sash1* in endothelial cells by crossing *Sash1*$^{fl/fl}$ mice with vascular endothelial (VE)-Cadherin-Cre (VEC-Cre) mice (Chen et al., 2009) to generate VEC-Cre-*Sash1*$^{fl/fl}$ embryos. Similar to *Sash1*$^{-/-}$ embryos, mRNA levels of all surfactant-associated proteins was significantly lower in VEC-Cre-*Sash1*$^{fl/fl}$ embryos compared to WT littermates at E18.5 (Figure 2E), supporting the hypothesis that Sash1 is required in the endothelium for AE2 cell maturation and surfactant production.

To further investigate the effect of *Sash1* in endothelial cells, we performed microarray analysis of E18.5 CD31^{+} lung endothelial cells isolated by fluorescence-activated cell sorting (FACS) from WT and *Sash1*$^{-/-}$ embryos. These data were compared to expression data from normal developing lung to assess whether the immature phenotype observed could be more widely generalized, including the endothelium. We analyzed custom gene sets made from pairwise comparisons of lung differentially expressed genes during lung development (Beauchemin et al., 2016; Xu et al., 2012). The gene signature of *Sash1*$^{-/-}$ lungs was enriched in genes associated with an earlier developmental time point when compared to WT (Figure 3A). Specifically, the transcriptome of E18.5 *Sash1*$^{-/-}$ endothelial cells correlated with genes typically overexpressed in lung at E17 compared to E18 (Figure 3A), whereas the expression pattern in WT cells was concordant with E18 lungs (Figure 3B). Similarly, genes normally downregulated during the canalicular (E16.5–E17.5) to saccular (E18.5–postnatal) transition were still enriched in *Sash1*$^{-/-}$ embryos (Figure 3A). This is an important observation given that the saccular stage of development is characterized by the differentiation of AE1 and AE2 cells during the perinatal period in mice (Woik and Kroll, 2015). Therefore, the microarray data point toward a lung maturation delay that originates from the endothelium and impacts AE2 cells and potentially AE1 cells. As a result of this finding, we examined the expression of two AE1 markers, *Pdpn* and *Aqp5*, by qRT-PCR. Expression of the AE1 cell marker *Aqp5* was lower in *Sash1*$^{-/-}$ embryos compared to WT littermates (Figure 3C), while *Pdpn* expression was, on average, not significantly altered at the mRNA level in *Sash1*$^{-/-}$ lungs, with the data showing more variation between samples (Figure 3C). This difference in *Aqp5* expression was also noted in VEC-Cre-*Sash1*$^{fl/fl}$ embryos when compared to WT littermates (Figure 3D). In the endothelial-specific knockouts a difference in *Pdpn* expression was also noted (Figure 3D). The fact that *Pdpn* expression did not always correlate with *Aqp5* could be due to slightly different expression patterns during development (Desai et al., 2014; Flodby et al., 2010). Given that some bipotent progenitor cells express *Pdpn*, it may be that *Pdpn* is upregulated earlier than *Aqp5* during AE1 differentiation (Desai et al., 2014). Nevertheless, these findings indicate that the effect of *Sash1* loss is a more generalized lung maturation delay rather than a deficiency in cell number or lung structure, and is dependent on endothelial *Sash1* expression.

Sash1 Interacts with β-Arrestin 1 to Activate Akt and eNOS

Given that SASH1 contains several motifs that mediate protein-protein interactions, we used a yeast-two-hybrid approach, using the full-length human SASH1 protein as bait, to identify SASH1-interacting proteins. A wide range of nuclear and cytoplasmic interacting proteins were identified, with β-arrestin 1 being the highest-confidence SASH1 interactor (Table S1). Interestingly, β-arrestin 1 and β-arrestin 2 double-deficient mice (*Arrb1*$^{-/-}$*Arrb2*$^{-/-}$) display a similar phenotype to *Sash1*$^{-/-}$ mice, including reduced surfactant protein expression (Zhang et al., 2010). To validate the interaction of Sash1 with β-arrestin 1, we transiently transfected cells with Flag-SASH1 and HA-β-arrestin 1 and confirmed by reciprocal co-immunoprecipitation (coIP) that SASH1 is found in a complex with β-arrestin 1 (Figure 4A).

To define the pathways that *Sash1* activates in endothelial cells, we used gene set enrichment analysis (GSEA) and examined pathways enriched in E18.5 WT endothelial cells compared to *Sash1*$^{-/-}$ endothelial cells from the microarray gene expression

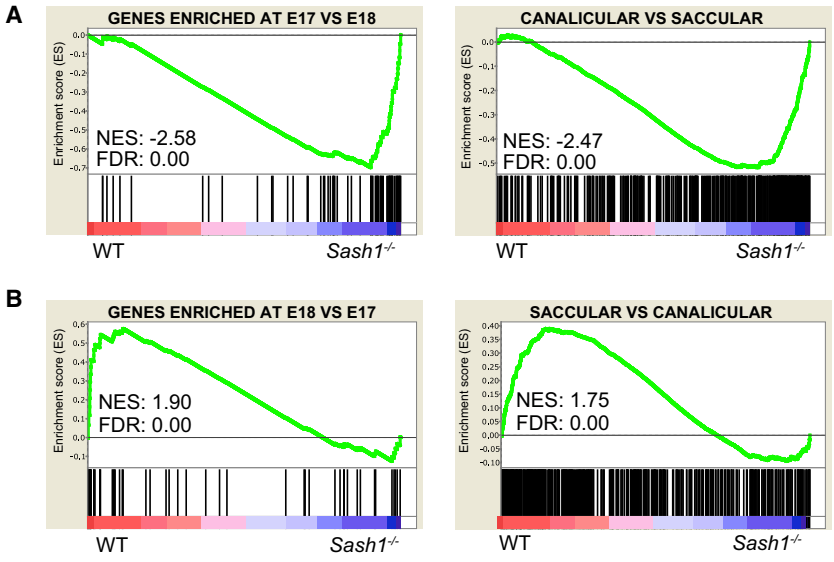

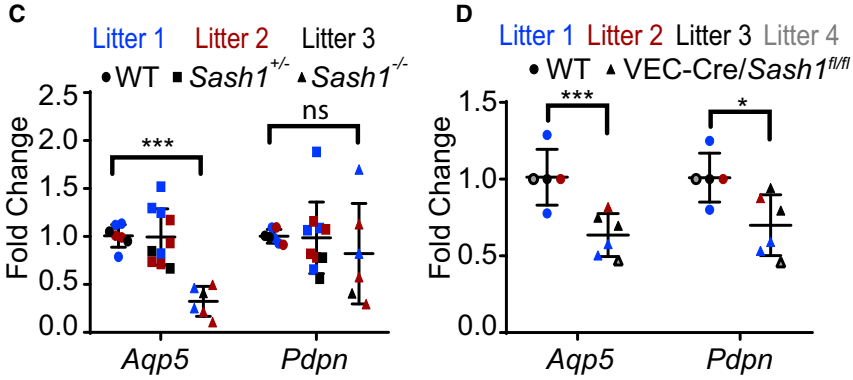

Figure 3. Gene Expression Reflects a Maturation Delay in *Sash1*$^{-/-}$ Lungs

(A) Enrichment plots of genes overexpressed at earlier developmental stages comparing E17 to E18 lungs, and genes differentially expressed between the canalicular and saccular stages showing an immature phenotype.

(B) Enrichment plots of genes upregulated in an E18 lung compared to E17 and upregulated during the transition to the saccular stage of development during normal maturation.

(C and D) Expression of AE1 cell markers *Aqp5* and *Pdpn* mRNA transcripts, by qRT-PCR, in E18.5 lungs. Data normalized to *Gapdh* represented as fold-change compared to WT littermates, shown as mean ± SD (n = 7 WT, 10 *Sash1*$^{+/-}$, and 6 *Sash1*$^{-/-}$ in C and n = 5 WT and 6 VEC-Cre-*Sash1*$^{fl/fl}$ in D) (*p < 0.05, **p < 0.01, ***p < 0.001). Each symbol color in (C) and (D) represents mice derived from the same litter.

See also Figures S3 and S4.

data presented above. As expected, GSEA analysis found that genes induced by ARRB1 overexpression were overrepresented in WT lung endothelium (Figure 4B), whereas repressed genes from this gene set overlapped with genes upregulated in *Sash1*$^{-/-}$ cells (Figure 4C; Tables S2 and S3) (Zecchini et al., 2014). This is consistent with the hypothesis that β-arrestin-1-directed transcriptional activity is repressed in *Sash1*$^{-/-}$ cells. GSEA analysis also identified several pathways associated with NF-κB and innate immune signaling (Figures 4D and 4E; Tables S2 and S3), as anticipated given the role of Sash1 in TLR4 signaling (Dauphinee et al., 2013). Intriguingly, this analysis also identified Akt and NO-related pathways as being repressed in *Sash1*$^{-/-}$ endothelial cells (Figures 4F and 4G). Akt is required for alveolar and AE2 cell development (Alphonse et al., 2011), and activated Akt activates eNOS through phosphorylation of Ser1177, which in turn leads to an increase in NO production (Dimmeler et al., 1999). In contrast, other endothelial signaling pathways previously shown to be implicated in alveolar maturation, vascular endothelial growth factor receptor (VEGFR) and FGFR (Ding et al., 2011), were not affected by loss of *Sash1* (Figures 4H and 4I; Tables S2 and S3), leading us to further explore the implication of an Akt-eNOS pathway in Sash1-driven lung development.

To determine whether Sash1 regulates Akt-eNOS downstream of the TLR4 receptor, we used lentiviral-delivered small hairpin RNA (shRNA) to knock down the expression of *SASH1*. Cells were subsequently treated with LPS, a ligand known from previous studies to activate *SASH1 in vitro* (Dauphinee et al., 2013). Knockdown of *SASH1* followed by LPS stimulation in human microvascular endothelial cells (HMECs) led to a significant decrease in phosphorylation of both Akt and eNOS (Figure 5A). Similarly, LPS stimulation of *Arrb1/2* double-null murine embryonic fibroblasts showed that β-arrestin is required to activate Akt, through phosphorylation of Ser473, downstream of TLR4 (Figure 5B). To determine the effect of abrogated Akt activation on the phosphorylation of eNOS and investigate the requirement of β-arrestin 1 and SASH1 interaction in this pathway, HMECs were transduced with shRNA specific for *ARRB1*. Following LPS stimulation, phosphorylation of both Akt and eNOS was decreased in *ARRB1* knockdown HMEC, compared to controls (Figure 5C), as seen with *SASH1* knockdown (Figure 5A). To confirm that NO production was reduced following *SASH1* knockdown, human lung microvascular endothelial cells (HMVECs-L) were transduced with shRNA targeting *SASH1* and stimulated with LPS. NO production was significantly decreased compared to control, as measured by the Griess reaction (Figure 5D). We have previously shown that PI3K and Akt inhibitors prevent the activating phosphorylation of the eNOS Ser1177 residue in HMEC (Chang et al., 2011), suggesting that Sash1 and β-arrestin act through Akt to activate eNOS and generate NO in pulmonary endothelial cells.

To assess whether the interaction between Sash1 and β-arrestin1 is critical to activating this pathway, we first investigated their cognate interacting domains by using deletion mutants

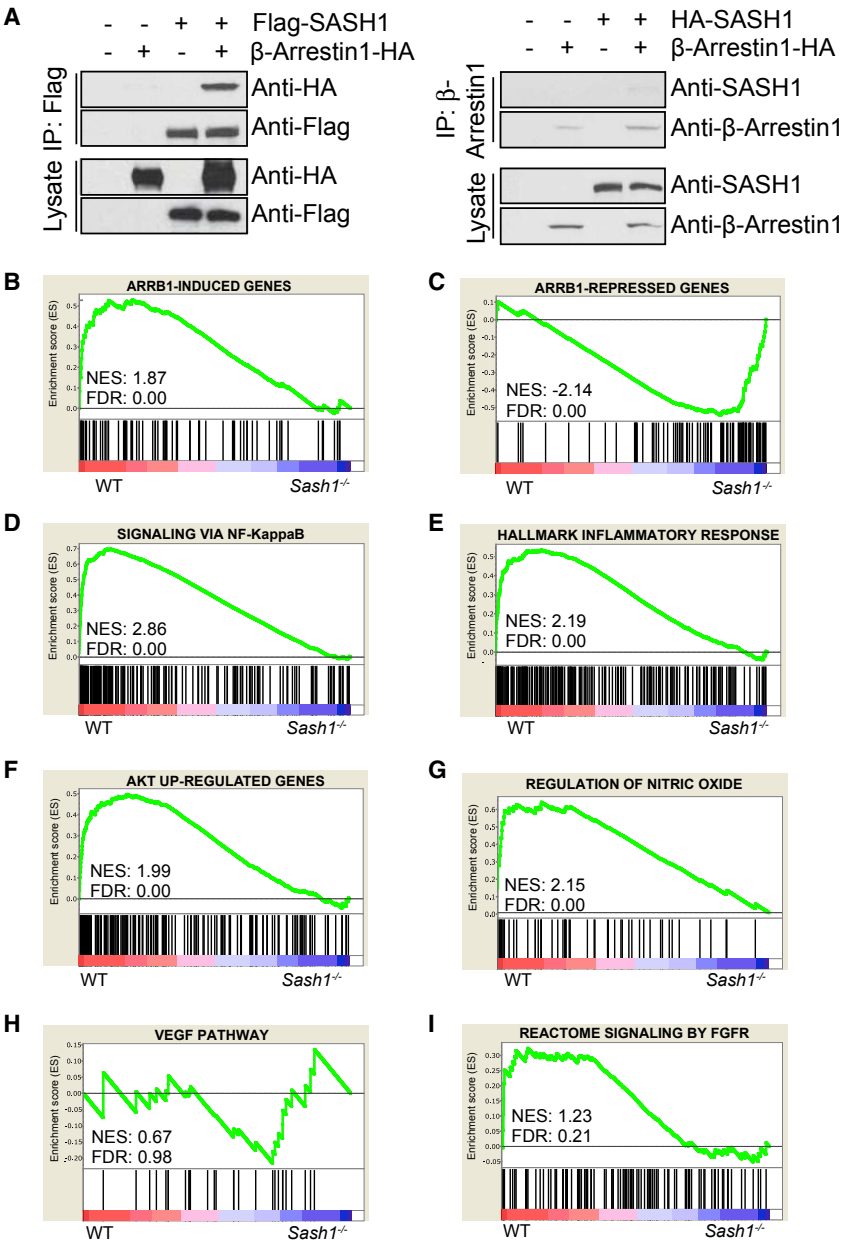

Figure 4. Pathways Affected by Loss of *Sash1* in E18.5 Pulmonary Endothelial Cells

(A) Lysates from HEK293T cells co-transfected with Flag-SASH1 or HA-SASH1, as indicated, and HA-tagged β-arrestin 1 were immunoprecipitated (IP) with anti-Flag, anti-Arrb1, or anti-HA antibodies, as indicated. Interactions were monitored by immunoblotting with anti-HA, anti-SASH1, or anti-Flag, as indicated. Empty vector (-) was used as control.

(B–I) Enrichment plots of selected gene sets based on gene set enrichment analysis (GSEA) using microarray data from E18.5 WT and *Sash1*$^{-/-}$ endothelial cells.

(B and C) β-arrestin 1-induced genes are over-represented in WT (B), while genes repressed by β-arrestin 1 are enriched in *Sash1*$^{-/-}$ (C).

(D–G)Enrichment of gene sets related to immune signaling via NK-κB (D), inflammatory response (E), Akt (F), and NO pathways (G) in WT compared to *Sash1*$^{-/-}$.

(H and I) Gene sets related to VEGF (H) and FGF (I) signaling are unaffected by *Sash1* knockout.

See also Tables S1, S2, and S3.

that lack the characterized SH3 (SASH1ΔSH3) or SAM1 (SASH1-ΔSAM1) domains of SASH1 and the N terminus or C terminus of β-arrestin 1 (Figure S5). coIP experiments revealed that the first SAM domain (SAM1) of SASH1 and the C-terminal domain of β-arrestin 1 are required for their interaction (Figure S5). Therefore, we used mutant constructs expressing only their cognate interacting domains to act as dominant-negative proteins and assessed the effect on AKT-eNOS activation. Overexpression of either the C-terminal domain of β-arrestin1 (amino acid 319-418) that binds Sash1 or of the Sash1 SAM1 domain, which binds β-arrestin1, prevented activation of Akt and eNOS following LPS stimulation in HMEC (Figure 5E). These observations suggest that the interaction of functional Sash1 and β-arrestin1 is required to activate the Akt-eNOS pathway. Together these data support a role for Sash1 and β-arrestin 1 interaction in activating Akt and eNOS downstream of TLR4 in pulmonary endothelial cells.

The Sash1-Akt Signaling Axis in Endothelial Cells Promotes Maturation of AE1 and AE2 Cells through Release of NO

To address the role of NO downstream of Sash1-β-arrestin 1-Akt-eNOS activation in lung maturation and surfactant production, pregnant mice were administered diaminorhodamine 4M-AM (DAR4M-AM), which forms NO adducts *in vivo*, intraperitoneally 1 h before harvesting embryonic lungs at E17.5. A significant decrease in DAR4M-AM co-staining with endothelial cells was observed in *Sash1*$^{-/-}$ lungs compared to WT littermates (Figures 6A and 6B), supporting a role for Sash1 in mediating endothelial NO production. Similarly, DAR4M-AM staining was significantly reduced in VEC-Cre-*Sash1*$^{fl/fl}$ embryos, further supporting that NO is mainly produced downstream of Sash1 in endothelial cells (Figures 6C and 6D). To assess whether endothelial NO had an effect on AE2 cells, we examined the AE2-enriched population of EpCAM^{+}T1α^{lo} cells by flow cytometry (Figure S4) after DAR4M-AM injection. The geometric mean fluorescence intensity (gMFI) of DAR4M-AM was decreased in EpCAM^{+}T1α^{lo} cells from VEC-Cre-*Sash1*$^{fl/fl}$ lungs (gMFI = 257.7 ± 8.9) compared to WT (gMFI = 289.3 ± 3.8) ($p = 0.03$) (Figure S6). Given the endothelial-restricted deletion of Sash1 in these animals, this observation points to an endothelial origin of NO signaling to adjacent epithelial cells. Interestingly, we observed a similar deficiency in lung

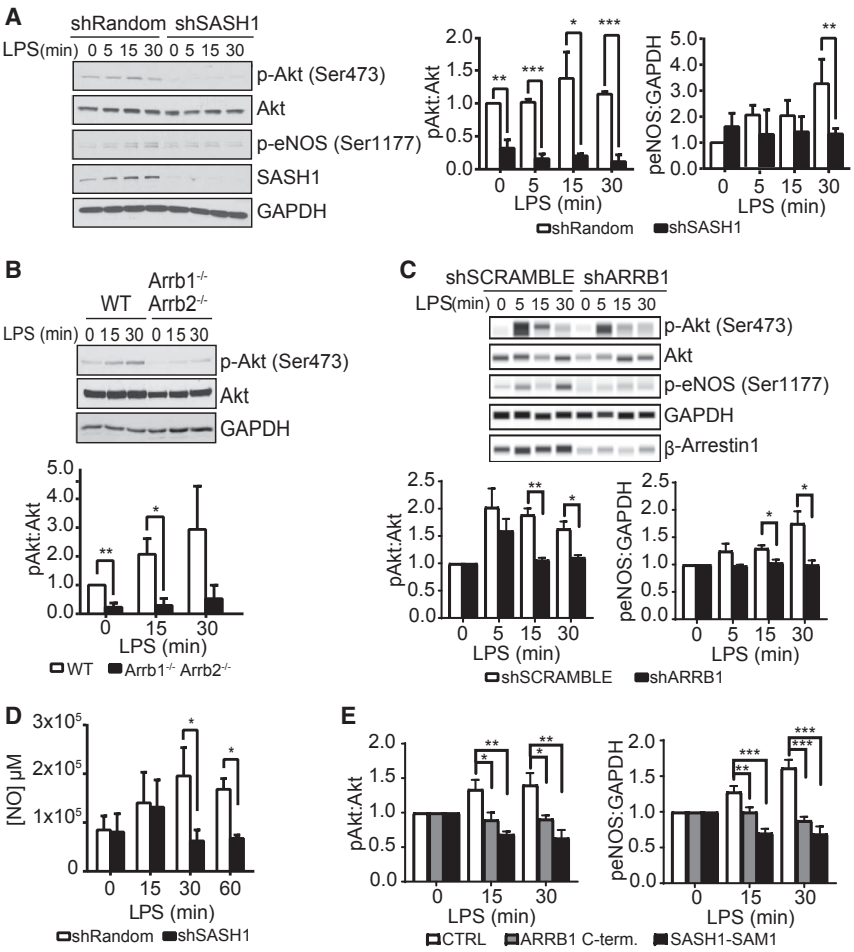

Figure 5. SASH1 and β-Arrestin 1 Induce NO through an Akt-eNOS Pathway

(A) HMEC were transduced with shRNA specific for SASH1 and induced with 100 ng/mL LPS. Phosphorylation of Akt (Ser473) and eNOS (Ser1177) was analyzed by immunoblotting of cell lysates following LPS stimulation. Densitometric scans of the bands from the western blot were performed to quantify phosphoprotein levels of Akt and eNOS normalized to total Akt or GAPDH, respectively.

(B) Wild-type or *Arrb1*$^{-/-}$*Arrb2*$^{-/-}$ mouse embryonic fibroblasts (MEFs) were stimulated with LPS (100 ng/mL) for the indicated times and lysates were immunoblotted with antibodies against phospho-Akt (Ser473) and total Akt. Lysates were also immunoblotted with anti-GAPDH as a loading control. Densitometric scans of the bands from blot were performed and phosphoprotein levels were normalized to the expression of total Akt protein.

(C) HMEC were transduced with shRNA specific for β-arrestin 1 and induced with 100 ng/mL LPS. Phosphorylation of Akt (Ser473) and eNOS (Ser1177) was analyzed by capillary immunoassay and quantification was performed using the area under the peak (n = 3).

(D) NO levels in shSASH1-transduced HMVEC-L were quantified by Griess reaction and compared to shRandom control.

(E) HMEC were transduced with constructs expressing only the SAM1 domain of SASH1 (aa 633-697), the C terminus of β-arrestin 1 (aa 319-418), or empty vector (CTRL). Phosphorylation of Akt (Ser473) and eNOS (Ser1177) was analyzed following LPS stimulation (100 ng/mL) using capillary immunoassay. Quantification was performed using the area under the peak (n = 5 CTRL, 4 ARRB1 C-term, and 4 SASH1-SAM1). Data are presented as mean ± SEM (*p < 0.05, **p < 0.01, ***p < 0.001). See also Figure S5.

surfactant protein production in *eNOS*$^{-/-}$ mice at E17.5, indicating a role for endothelial-derived NO in promoting surfactant protein production (Figure S7).

Since NO is known to signal through sGC and to demonstrate a direct effect of NO signaling on AE2 cells, we investigated the effect of both NO and sGC activation on FACS-isolated AE2 cells *in vitro* using chemical treatment. Cells were sorted from *Sash1*$^{-/-}$ lungs, at the time of birth, to exclude endothelial cells and enrich for alveolar epithelial cells (Figure S4), then plated and treated overnight with either the nitric oxide donor S-Nitroso-N-acetylpenicillamine (SNAP) or the sGC activator BAY41-2272. Both BAY41-2272 and SNAP treatment increased SP-B and SP-C transcript levels in isolated AE2 cells compared to DMSO or PBS controls (Figures 7A and 7B), supporting the idea that endothelial-derived NO acts on AE2 cells in an sGC-dependent manner to drive surfactant production. Given that sGC activation showed increased surfactant transcripts *in vitro*, we investigated whether blocking this pathway in WT mice would result in a phenotype similar to *Sash1*$^{-/-}$ animals. Following intraperitonal administration of the sGC inhibitor 1H-[1,2,4]Oxadiazolo[4,3-a]quinoxalin-1-one (ODQ) at E17.5, E18.5 surfactant transcript levels were significantly reduced in the ODQ-treated WT embryos compared to vehicle-treated WT embryos. However, there was no difference between ODQ- and vehicle-treated *Sash1*$^{-/-}$ embryos (Figure 7C). Thus, ODQ treatment in WT embryos mimics the *Sash1*$^{-/-}$ defect, while further inhibition of sGC has no impact on surfactant production in *Sash1*$^{-/-}$ embryos.

To determine whether an NO donor could bypass *Sash1* deficiency *in vivo*, mice were given SNAP intraperitoneally 24 h before harvesting embryos. *Sash1*$^{-/-}$ embryos from mice that received SNAP treatment showed normalization of surfactant-associated protein transcript levels (Figure 7D) at E18.5. Interestingly, surfactant synthesis was reduced in WT animals that received SNAP suggestive of a dose-dependent effect of NO. Excessive nitric oxide has been shown to induce nitrosative stress that can lead to cell death (Moldogazieva et al., 2018). In addition, we observed a similar effect of SNAP treatment on AE1 markers (Figure 7E), suggesting that endothelial-derived NO may drive general epithelial cell maturation. Similarly, activation of sGC *in vivo* using Riociguat (BAY63-2521), an sGC activator that acts independently of NO, normalized surfactant transcript levels (Figure 7F) and *Aqp5* expression (Figure 7G) compared to vehicle-treated *Sash1*$^{-/-}$. These data suggest that NO is important in lung epithelial cell maturation leading to surfactant synthesis and supports the idea that the developmental defect in *Sash1*$^{-/-}$ embryos originates from deficient eNOS activation.

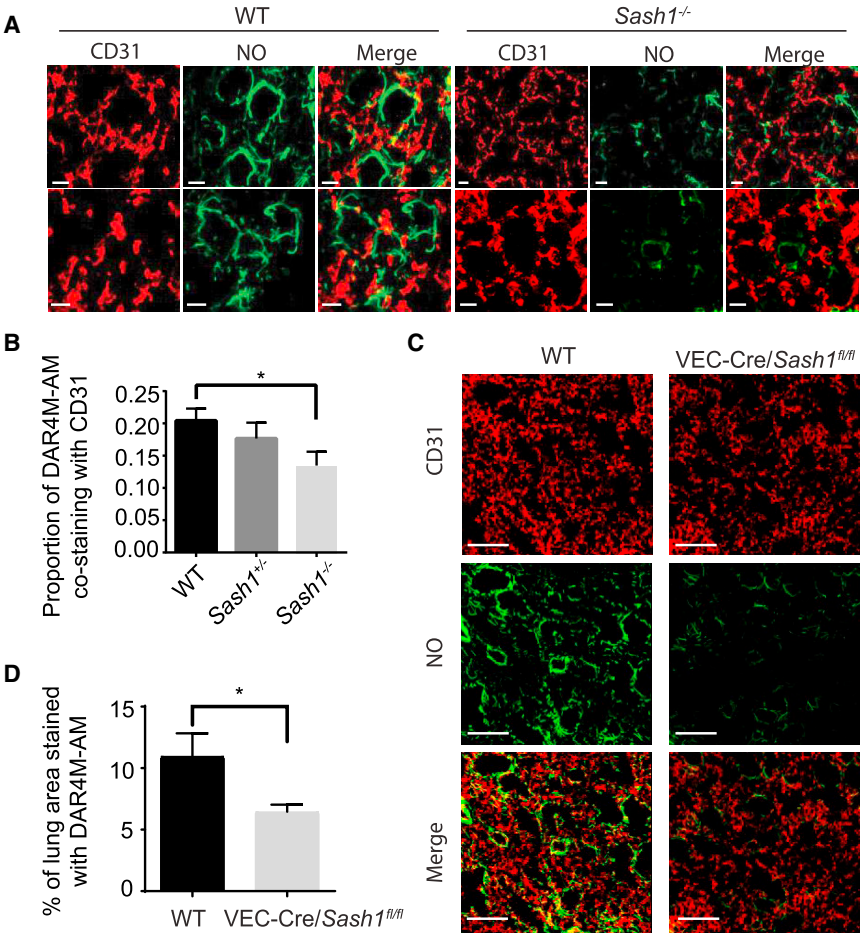

Figure 6. Sash1 Deficiency Reduces NO Production from the Lung Endothelium

Pregnant mice were administered DAR4M-AM intraperitoneally (25 μmol/kg) 1 h prior to harvesting the embryos at E17.5.

(A and C) Lung sections were analyzed by immunofluorescence for NO (green) and CD31 (red) in (A) *Sash1*$^{-/-}$ or (C) VEC-Cre-*Sash1*$^{fl/fl}$ and wild-type (WT) littermates.

(B) Quantification of DAR4M-AM and CD31 co-staining in WT (n = 4) lungs compared to *Sash1*$^{+/-}$ (n = 5) and *Sash1*$^{-/-}$ (n = 9) lungs.

(D) Quantification of DAR4M-AM positive pixels as a fraction of surface area in the lung of VEC-Cre-*Sash1*$^{fl/fl}$ (n = 4) compared to WT littermates (n = 3). Data are presented as mean ± SEM (*$p < 0.05$). Scale bars: 20 μm in (A) and 100 μm in (C). See also Figure S6.

DISCUSSION

Late-stage alveolar maturation is essential to survival at birth and preterm delivery is often associated with respiratory distress in humans (Woik and Kroll, 2015). Maturation of AE2 cells is one of the major changes occurring in the lungs before birth and leads to secretion of surfactant B and C by AE2 cells in order to reduce alveolar surface tension (Young et al., 1991). Investigation of the neonatal lethality observed in *Sash1*$^{-/-}$ mice revealed an immature lung phenotype characterized by AE2 cells lacking lamellar bodies, a defect in surfactant-associated protein synthesis, and reduced expression of AE1 specific cell markers.

Conditional deletion of *Sash1* in the endothelium resulted in a similar defect in expression of mature alveolar cell markers, confirming a role for the endothelium in this process. Given the highly structured network of the lung, it is not surprising that alveolar development is coupled with blood vessel formation (Woik and Kroll, 2015). Inhibition of endothelial cell migration alone, by blocking platelet endothelial cell adhesion molecule 1 (PECAM-1), disrupts normal alveolar septation, resulting in larger tubular structures, without affecting proliferation or survival of endothelial cells (DeLisser et al., 2006). However, *Sash1* loss has minimal if any impact on lung alveolar or endothelial structure. Rather, the defect appears to reside in signaling between the endothelium and alveolar epithelial cells. Ding et al. (2011) reported that the lung endothelium secretes angiocrine factors, such as VEGF, to promote alveolar growth, proliferation, and repair. However, in *Sash1*$^{-/-}$ lungs there was no difference in VEGFR signaling seen in our transcriptome analysis. The fact that no difference was observed in cell-type composition or lung morphology in *Sash1*$^{-/-}$ embryos compared to WT littermates is consistent with a signaling defect rather than a growth or alveolarization defect.

We have previously described SASH1 as a scaffold protein in innate immunity downstream of TLR4 (Dauphinee et al., 2013). Scaffold molecules are known to interact with many binding partners to regulate signaling. Here, we show that SASH1 interacts with β-arrestin 1 and this interaction appears to play a critical role in lung endothelial signaling. Constitutive knockout of β-arrestins, as previously described in *Arrb1*$^{-/-}$*Arrb2*$^{-/-}$ animals, results in a surfactant defect similar to *Sash1*$^{-/-}$ mice although a mechanism was not identified in the *Arrb1*$^{-/-}$*Arrb2*$^{-/-}$ animals (Zhang et al., 2010). TLR4-induced NF-κB activation requires TRAF6 (Dauphinee et al., 2013; Wi et al., 2014), but we demonstrate that β-arrestin interacts with a SASH1 domain distinct from the TRAF6 binding domain, consistent with a TRAF6 and NF-κB-independent effect of SASH1 in lung development.

Downstream of Sash1 and β-arrestin-1, our findings indicate that Akt activation phosphorylates eNOS to promote NO release. Our model suggests that endothelial-expressed Sash1 acts to regulate NO production, and that NO can signal to epithelial cells to promote parenchymal cell maturation. Our *in vitro* experiments support that NO can directly affect AE2 cells; however, we cannot exclude the possibility of interactions with other cells types to induce maturation. While our study focused on the endothelial cells expressing Sash1, released NO could be signaling to epithelial cells both directly and

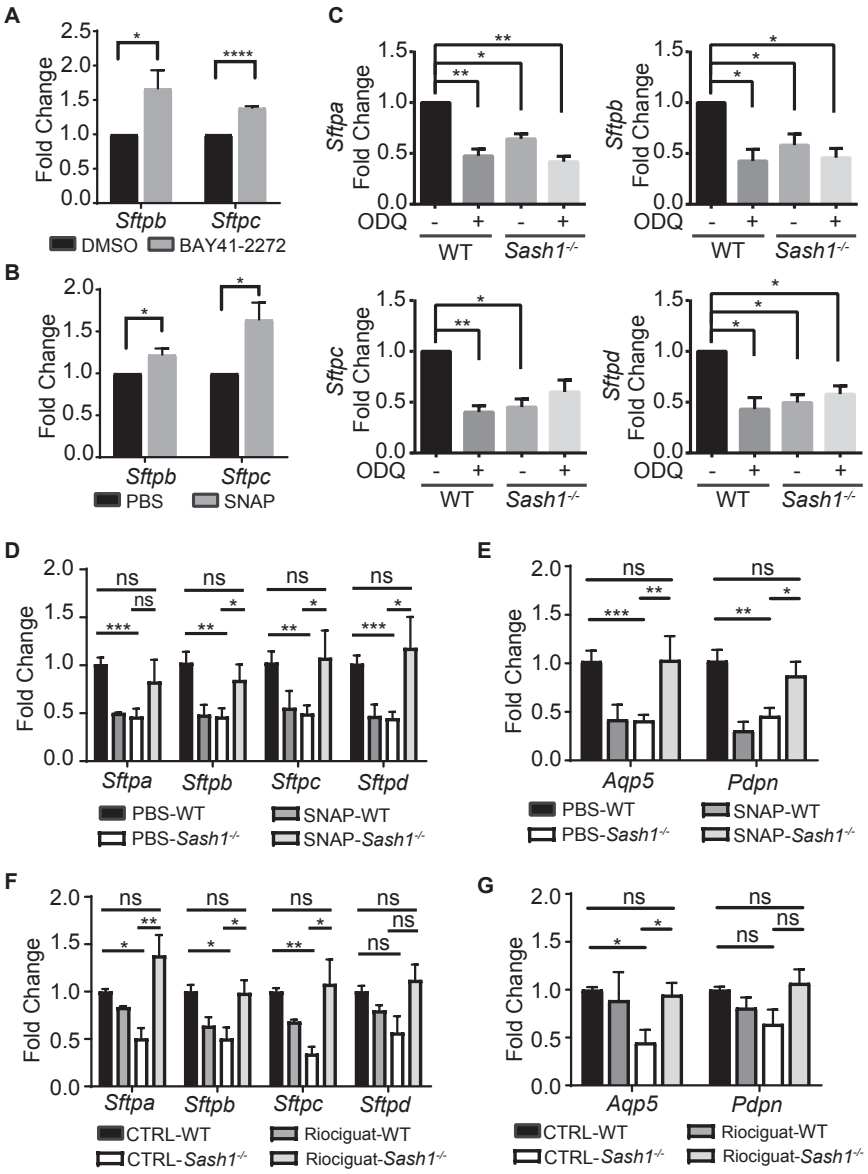

Figure 7. Sash1 Promotes Maturation of Alveolar Epithelial Cells through the NO-cGMP Pathway

(A and B) FACS-isolated AE2 cells (see Figure S4) from neonatal lungs (P0) were treated with 10 μg/ml BAY41-2272 or DMSO (A) or 1 mM SNAP or PBS (B). Total RNA was extracted and SP-B and SP-C expression was quantified by digital droplet PCR (n = 4 in A and 5 in B).

(C–G) Expression of surfactant-associated protein mRNA transcripts (C, D, and F) and AE1 markers (E and G) in E18.5 lungs after treatment with 50 mg/kg ODQ (C), 5 mg/kg SNAP (D and E), or 10 mg/kg Riociguat (F and G) 24 h prior to harvesting the embryos. qRT-PCR values were compared to control WT embryos treated with DMSO (C), PBS (D and E), or methylcellulose (F and G): n = 3 (WT; ODQ–), 3 (WT; ODQ+), 3 (*Sash1*$^{-/-}$; ODQ–), 5 (*Sash1*$^{-/-}$; ODQ+) in (C); n = 5 (PBS-WT), 10 (PBS-*Sash1*$^{-/-}$), 3 (SNAP-WT), and 5 (SNAP-*Sash1*$^{-/-}$) in (D and E); and n = 3 (CTRL-WT), 5 (CTRL-*Sash1*$^{-/-}$), 3 (Riociguat-WT), and 4 (Riociguat-*Sash1*$^{-/-}$) in (F and G). Surfactant expression was normalized to *Gapdh*. Data are presented as mean ± SEM (*p < 0.05, **p < 0.01, ***p < 0.001). See also Figures S4 and S7.

indirectly via the mesenchyme (Habermehl et al., 2011). Administration of an NO-donor or sGC activator was able to restore the surfactant level in *Sash1*$^{-/-}$ mice, confirming the role of NO in this process. This signaling cascade is consistent with our previous demonstration of a TRAF6-independent pathway to activate Akt downstream of TLR4 (Dauphinee et al., 2011). Interestingly, *eNOS*$^{-/-}$ mice are also born with respiratory distress, but a defect in alveolar surfactant-associated protein production was not described (Han et al., 2004). An *eNOS* deficiency was also reported to impair angiogenesis, which we did not observe in *Sash1*$^{-/-}$ animals, suggesting that eNOS depletion in non-endothelial cells may be contributing to the phenotype in *eNOS*$^{-/-}$ mice (Han et al., 2004; Sherman et al., 1999; Sood et al., 2011).

NO acts as a signaling molecule via a cyclic guanosine monophosphate (cGMP)-dependent mechanism. Activation of sGC by NO induces the conversion of GTP into cGMP which stimulates cGMP-dependent protein kinase (PKG) (Francis et al., 2010). Our data demonstrate that inhibition of sGC activity with ODQ impairs surfactant-associated protein synthesis in WT animals to levels comparable to *Sash1*$^{-/-}$ mice. Conversely, an sGC activator stimulated SP-C production, which was used as a marker for AE2 cell maturation. While we focused our study on the signaling of NO to activate sGC and regulate surfactant transcription, nitrosylation of surfactant-associated proteins by NO has been reported to modulate immune responses (Guo et al., 2008). Specifically, nitrosylation of SP-D has been suggested to impair its inhibitory effect on Tlr4 (Guo et al., 2008). It will be of interest to further define the role of nitrosylation during lung development.

Respiratory distress syndrome, secondary to alveolar immaturity and surfactant defects, is one of the major causes of morbidity and mortality in preterm newborns, resulting in death or progression to bronchopulmonary dysplasia, the most common severe complication of preterm birth (Ainsworth, 2005; Jobe, 2011; Read et al., 2016). Although management has become routine, optimized and less invasive treatment strategies could derive from an understanding of the developmental and pathophysiological processes contributing to lung immaturity. Together, our findings connect immune signaling downstream of TLR4 to NO signaling, defining a pathway involved in embryonic lung development leading to the initiation of surfactant secretion by mature AE2 cells, and outline the importance

of interactions between the endothelium and epithelium during alveolar development.

STAR★METHODS

Detailed methods are provided in the online version of this paper and include the following:

- KEY RESOURCES TABLE
- CONTACT FOR REAGENT AND RESOURCE SHARING
- EXPERIMENTAL MODEL AND SUBJECT DETAILS
  - Mice
  - Cell Lines
- METHOD DETAILS
  - H&E/PAS/IHC
  - RNA, qRT-PCR, and ddPCR
  - Flow Cytometry
  - Microarray and Bioinformatics
  - Recombinant Plasmids, Gene Transfer, and RNA interference
  - Co-Immunoprecipitation, Immunoblotting, and Immunoassay
  - DAR4M-AM Staining
  - *In Vitro* AE2 Cell Assay
- QUANTIFICATION AND STATISTICAL ANALYSIS
- DATA AND SOFTWARE AVAILABILITY

SUPPLEMENTAL INFORMATION

Supplemental Information can be found online at https://doi.org/10.1016/j.celrep.2019.04.039.

ACKNOWLEDGMENTS

We thank Derrick Horne at the UBC Bioimaging facility for his assistance with the TEM and Dr. David C. Walker for helpful discussions regarding lung development. This work was supported by grants from the Canadian Institutes for Health Research to A.K. P.C. and A.H. were supported by a Canadian Institutes for Health Research studentship and a University of British Columbia doctoral fellowship. S.D. was supported by studentships from the Canadian Institutes for Health Research and the Michael Smith Foundation for Health Research. A.K. is the recipient of the John Auston BC Cancer Foundation Clinical Investigator Award.

AUTHOR CONTRIBUTIONS

P.C. and G.N.P. designed and performed research, analyzed and interpreted the data, and wrote the manuscript; A.C., M.F., and V.J. performed research; and S.D. and A.H. contributed to the experimental design. P.U. and M.F. were responsible for animal husbandry; P.X., R.K.H., and P.A.H. contributed to the generation of the mouse models; A.H.K., A.I.M., and J.L.W. contributed to the experimental design and data interpretation; and J.D.K.P. contributed to data analysis, interpretation, and manuscript preparation. A.K. conceived and designed the study, interpreted the data, and wrote the manuscript.

DECLARATION OF INTERESTS

The authors declare no competing interests.

Received: March 3, 2017
Revised: March 7, 2019
Accepted: April 5, 2019
Published: May 7, 2019

REFERENCES

Ainsworth, S.B. (2005). Pathophysiology of neonatal respiratory distress syndrome: implications for early treatment strategies. Treat. Respir. Med. *4*, 423–437.

Alphonse, R.S., Vadivel, A., Coltan, L., Eaton, F., Barr, A.J., Dyck, J.R., and Thébaud, B. (2011). Activation of Akt protects alveoli from neonatal oxygen-induced lung injury. Am. J. Respir. Cell Mol. Biol. *44*, 146–154.

Baker, J.H., Lam, J., Kyle, A.H., Sy, J., Oliver, T., Co, S.J., Dragowska, W.H., Ramsay, E., Anantha, M., Ruth, T.J., et al. (2008). Irinophore C, a novel nanoformulation of irinotecan, alters tumor vascular function and enhances the distribution of 5-fluorouracil and doxorubicin. Clin. Cancer Res. *14*, 7260–7271.

Beauchemin, K.J., Wells, J.M., Kho, A.T., Vivek, M.P., Kamir, D., Kohane, I.S., Graber, J.H., and Bult, C.J. (2016). Temporal dynamics of the developing lung transcriptome in three common inbred strains of laboratory mice reveals multiple stages of postnatal alveolar development. PeerJ *4*, e2318.

Bourbon, J.R., Rieutort, M., Engle, M.J., and Farrell, P.M. (1982). Utilization of glycogen for phospholipid synthesis in fetal rat lung. Biochim. Biophys. Acta *712*, 382–389.

Carreto-Binaghi, L.E., Aliouat, M., and Taylor, M.L. (2016). Surfactant proteins, SP-A and SP-D, in respiratory fungal infections: their role in the inflammatory response. Respir. Res. *17*, 66.

Chang, A.C., Fu, Y., Garside, V.C., Niessen, K., Chang, L., Fuller, M., Setiadi, A., Smrz, J., Kyle, A., Minchinton, A., et al. (2011). Notch initiates the endothelial-to-mesenchymal transition in the atrioventricular canal through autocrine activation of soluble guanylyl cyclase. Dev. Cell *21*, 288–300.

Chen, M.J., Yokomizo, T., Zeigler, B.M., Dzierzak, E., and Speck, N.A. (2009). Runx1 is required for the endothelial to haematopoietic cell transition but not thereafter. Nature *457*, 887–891.

Cochrane, C.G., and Revak, S.D. (1991). Pulmonary surfactant protein B (SP-B): structure-function relationships. Science *254*, 566–568.

Dauphinee, S.M., and Karsan, A. (2006). Lipopolysaccharide signaling in endothelial cells. Lab. Invest. *86*, 9–22.

Dauphinee, S.M., Voelcker, V., Tebaykina, Z., Wong, F., and Karsan, A. (2011). Heterotrimeric Gi/Go proteins modulate endothelial TLR signaling independent of the MyD88-dependent pathway. Am. J. Physiol. Heart Circ. Physiol. *301*, H2246–H2253.

Dauphinee, S.M., Clayton, A., Hussainkhel, A., Yang, C., Park, Y.J., Fuller, M.E., Blonder, J., Veenstra, T.D., and Karsan, A. (2013). SASH1 is a scaffold molecule in endothelial TLR4 signaling. J. Immunol. *191*, 892–901.

DeLisser, H.M., Helmke, B.P., Cao, G., Egan, P.M., Taichman, D., Fehrenbach, M., Zaman, A., Cui, Z., Mohan, G.S., Baldwin, H.S., et al. (2006). Loss of PECAM-1 function impairs alveolarization. J. Biol. Chem. *281*, 8724–8731.

Desai, T.J., Brownfield, D.G., and Krasnow, M.A. (2014). Alveolar progenitor and stem cells in lung development, renewal and cancer. Nature *507*, 190–194.

Dimmeler, S., Fleming, I., Fisslthaler, B., Hermann, C., Busse, R., and Zeiher, A.M. (1999). Activation of nitric oxide synthase in endothelial cells by Akt-dependent phosphorylation. Nature *399*, 601–605.

Ding, B.-S., Nolan, D.J., Guo, P., Babazadeh, A.O., Cao, Z., Rosenwaks, Z., Crystal, R.G., Simons, M., Sato, T.N., Worgall, S., et al. (2011). Endothelial-derived angiocrine signals induce and sustain regenerative lung alveolarization. Cell *147*, 539–553.

Dobbs, L.G. (1989). Pulmonary surfactant. Annu. Rev. Med. *40*, 431–446.

Dobbs, L.G., and Johnson, M.D. (2007). Alveolar epithelial transport in the adult lung. Respir. Physiol. Neurobiol. *159*, 283–300.

Flodby, P., Borok, Z., Banfalvi, A., Zhou, B., Gao, D., Minoo, P., Ann, D.K., Morrisey, E.E., and Crandall, E.D. (2010). Directed expression of Cre in alveolar epithelial type 1 cells. Am. J. Respir. Cell Mol. Biol. *43*, 173–178.

Francis, S.H., Busch, J.L., Corbin, J.D., and Sibley, D. (2010). cGMP-dependent protein kinases and cGMP phosphodiesterases in nitric oxide and cGMP action. Pharmacol. Rev. *62*, 525–563.

Große Ostendorf, A.L., Rothschild, M.A., Müller, A.M., and Banaschak, S. (2013). Is the lung floating test a valuable tool or obsolete? A prospective autopsy study. Int. J. Legal Med. *127*, 447–451.

Guo, C.J., Atochina-Vasserman, E.N., Abramova, E., Foley, J.P., Zaman, A., Crouch, E., Beers, M.F., Savani, R.C., and Gow, A.J. (2008). S-nitrosylation of surfactant protein-D controls inflammatory function. PLoS Biol. *6*, e266.

Habermehl, D., Parkitna, J.R., Kaden, S., Brügger, B., Wieland, F., Gröne, H.J., and Schütz, G. (2011). Glucocorticoid activity during lung maturation is essential in mesenchymal and less in alveolar epithelial cells. Mol. Endocrinol. *25*, 1280–1288.

Han, R.N., Babaei, S., Robb, M., Lee, T., Ridsdale, R., Ackerley, C., Post, M., and Stewart, D.J. (2004). Defective lung vascular development and fatal respiratory distress in endothelial NO synthase-deficient mice: a model of alveolar capillary dysplasia? Circ. Res. *94*, 1115–1123.

Hillman, N.H., Moss, T.J.M., Nitsos, I., Kramer, B.W., Bachurski, C.J., Ikegami, M., Jobe, A.H., and Kallapur, S.G. (2008). Toll-like receptors and agonist responses in the developing fetal sheep lung. Pediatr. Res. *63*, 388–393.

Hsia, C.C., Hyde, D.M., and Weibel, E.R. (2016). Lung Structure and the Intrinsic Challenges of Gas Exchange. Compr. Physiol. *6*, 827–895.

Jobe, A.H. (2011). The new bronchopulmonary dysplasia. Curr. Opin. Pediatr. *23*, 167–172.

Jobe, A.H., and Goldenberg, R.L. (2018). Antenatal corticosteroids: an assessment of anticipated benefits and potential risks. Am. J. Obstet. Gynecol. *219*, 62–74.

Kuroki, Y., and Voelker, D.R. (1994). Pulmonary surfactant proteins. J. Biol. Chem. *269*, 25943–25946.

Lu, Y.-C., Yeh, W.-C., and Ohashi, P.S. (2008). LPS/TLR4 signal transduction pathway. Cytokine *42*, 145–151.

Moldogazieva, N.T., Mokhosoev, I.M., Feldman, N.B., and Lutsenko, S.V. (2018). ROS and RNS signalling: adaptive redox switches through oxidative/nitrosative protein modifications. Free Radical Res. *52*, 507–543.

Moss, T.J.M., and Westover, A.J. (2017). Inflammation-induced preterm lung maturation: lessons from animal experimentation. Paediatr. Respir. Rev. *23*, 72–77.

Perez-Gil, J., and Weaver, T.E. (2010). Pulmonary surfactant pathophysiology: current models and open questions. Physiology (Bethesda) *25*, 132–141.

Read, B., Lee, D.S., and Fraser, D. (2016). Evaluation of a practice guideline for the management of respiratory distress syndrome in preterm infants: A quality improvement initiative. Paediatr. Child Health *21*, e4–e9.

Rooney, S.A., Young, S.L., and Mendelson, C.R. (1994). Molecular and cellular processing of lung surfactant. FASEB J. *8*, 957–967.

Schellhase, D.E., and Shannon, J.M. (1991). Effects of maternal dexamethasone on expression of SP-A, SP-B, and SP-C in the fetal rat lung. Am. J. Respir. Cell Mol. Biol. *4*, 304–312.

Sherman, T.S., Chen, Z., Yuhanna, I.S., Lau, K.S., Margraf, L.R., and Shaul, P.W. (1999). Nitric oxide synthase isoform expression in the developing lung epithelium. Am. J. Physiol. *276*, L383–L390.

Sood, B.G., Wykes, S., Landa, M., De Jesus, L., and Rabah, R. (2011). Expression of eNOS in the lungs of neonates with pulmonary hypertension. Exp. Mol. Pathol. *90*, 9–12.

Warburton, D., El-Hashash, A., Carraro, G., Tiozzo, C., Sala, F., Rogers, O., De Langhe, S., Kemp, P.J., Riccardi, D., Torday, J., et al. (2010). Lung organogenesis. Curr. Top. Dev. Biol. *90*, 73–158.

Watterberg, K.L., Demers, L.M., Scott, S.M., and Murphy, S. (1996). Chorioamnionitis and early lung inflammation in infants in whom bronchopulmonary dysplasia develops. Pediatrics *97*, 210–215.

Weaver, T.E., and Conkright, J.J. (2001). Function of surfactant proteins B and C. Annu. Rev. Physiol. *63*, 555–578.

Wi, S.M., Moon, G., Kim, J., Kim, S.T., Shim, J.H., Chun, E., and Lee, K.Y. (2014). TAK1-ECSIT-TRAF6 complex plays a key role in the TLR4 signal to activate NF-κB. J. Biol. Chem. *289*, 35205–35214.

Willet, K.E., Kramer, B.W., Kallapur, S.G., Ikegami, M., Newnham, J.P., Moss, T.J., Sly, P.D., and Jobe, A.H. (2002). Intra-amniotic injection of IL-1 induces inflammation and maturation in fetal sheep lung. Am. J. Physiol. Lung Cell. Mol. Physiol. *282*, L411–L420.

Woik, N., and Kroll, J. (2015). Regulation of lung development and regeneration by the vascular system. Cell. Mol. Life Sci. *72*, 2709–2718.

Xu, Y., Wang, Y., Besnard, V., Ikegami, M., Wert, S.E., Heffner, C., Murray, S.A., Donahue, L.R., and Whitsett, J.A. (2012). Transcriptional programs controlling perinatal lung maturation. PLoS One *7*, e37046.

Young, S.L., Fram, E.K., Spain, C.L., and Larson, E.W. (1991). Development of type II pneumocytes in rat lung. Am. J. Physiol. *260*, L113–L122.

Zecchini, V., Madhu, B., Russell, R., Pértega-Gomes, N., Warren, A., Gaude, E., Borlido, J., Stark, R., Ireland-Zecchini, H., Rao, R., et al. (2014). Nuclear ARRB1 induces pseudohypoxia and cellular metabolism reprogramming in prostate cancer. EMBO J. *33*, 1365–1382.

Zeller, C., Hinzmann, B., Seitz, S., Prokoph, H., Burkhard-Goettges, E., Fischer, J., Jandrig, B., Schwarz, L.E., Rosenthal, A., and Scherneck, S. (2003). SASH1: a candidate tumor suppressor gene on chromosome 6q24.3 is downregulated in breast cancer. Oncogene *22*, 2972–2983.

Zhande, R., Dauphinee, S.M., Thomas, J.A., Yamamoto, M., Akira, S., and Karsan, A. (2007). FADD negatively regulates lipopolysaccharide signaling by impairing interleukin-1 receptor-associated kinase 1-MyD88 interaction. Mol. Cell. Biol. *27*, 7394–7404.

Zhang, M., Liu, X., Zhang, Y., and Zhao, J. (2010). Loss of betaarrestin1 and betaarrestin2 contributes to pulmonary hypoplasia and neonatal lethality in mice. Dev. Biol. *339*, 407–417.

STAR★METHODS

KEY RESOURCES TABLE

REAGENT or RESOURCE	SOURCE	IDENTIFIER
Antibodies		
Alexa Fluor®488 Anti-Mouse CD326 (EpCAM) [G8.8]	BioLegend	Cat# 118210, RRID:AB_1134099
Anti-Mouse CD45.2 APC-eFluor®780	eBioscience	Cat# 47-0454-82, RRID:AB_1272175
Anti-Mouse CD31 (PECAM-1) PerCP-eFluor®710	eBioscience	Cat# 46-0311-82, RRID:AB_1834429
APC anti-mouse Podoplanin	BioLegend	Cat# 127410, RRID:AB_10613649
Surfactant Protein B antibody	Abcam	Cat# ab3282, RRID:AB_2285683
Anti-Prosurfactant Protein C (proSP-C)	EMD Millipore	Cat# AB3786, RRID:AB_91588
Anti-beta Arrestin 1 antibody [E274]	Abcam	Cat# ab32099, RRID:AB_722896
SASH1 Antibody	Novus Biologicals	Cat# NBP1-26650, RRID:AB_1853473
HA.11 polyclonal antibody, purified	Covance	Cat# PRB-101P, RRID:AB_291552
β-Arrestin-2 Antibody (H-9)	Santa Cruz Biotechnology	Cat# sc-13140, RRID:AB_626701
Anti-Flag®M2	Sigma-Aldrich	Cat# M8823, RRID:AB_2637089
Monoclonal Anti-GAPDH antibody produced in mouse	Sigma-Aldrich	Cat# G8795, RRID:AB_1078991
Anti-GFP	Roche	Cat# 11814460001, RRID:AB_390913
Phospho-Akt (Ser473) (D9E) XP® Rabbit mAb	Cell Signaling Technology	Cat# 4060S, RRID:AB_2315049
Akt Antibody	Cell Signaling Technology	Cat# 9272S, RRID:AB_329827
Phospho-eNOS (S1177) Antibody	Cell Signaling Technology	Cat# 9571S, RRID:AB_329837
CD31 Monoclonal Antibody (2H8)	ThermoFisher	Cat# MA3105, RRID:AB_223592
Goat anti-Hamster IgG (H+L), Alexa Fluor 647	ThermoFisher	Cat# A-21451, RRID:AB_2535868
GAPDH (14C10) Rabbit mAb	Cell Signaling Technology	Cat# 2118S, RRID:AB_561053
Chemicals, Peptides, and Recombinant Proteins		
Riociguat (BAY63-2521)	Selleckchem	Cat# S8135
1H-[1,2,4]Oxadiazolo[4,3-a]quinoxalin-1-one (ODQ)	Sigma-Aldrich	Cat# O3636
Diaminorhodamine 4A-AM (DAR4M-AM)	Santa Cruz biotechnology	Cat# sc-221530
S-Nitroso-N-Acetyl-D,L-Penicillamine (SNAP)	Santa Cruz biotechnology	Cat# sc-200319B
Lipopolysaccharides from *Escherichia coli* 0111:B4	Sigma-Aldrich	Cat# L3024
BAY41-2272	Tocris Bioscience	Cat# 4430
Critical Commercial Assays		
Nitric Oxide Assay kit (Fluorometric)	Abcam	Cat# ab65327
Periodic Acid Schiff (PAS) Stain kit	Abcam	Cat# ab150680
*Trans*IT®-LT1 Transfection Reagent	Mirus	Product # MIR 2300
12-230 kDa Wes Separation Module	ProteinSimple	Cat# SM-W004
Deposited Data		
Raw and analyzed microarray data	This paper	GEO: GSE123889
Experimental Models: Cell Lines		
Human: HMEC-1	Centers for Disease Control and Prevention (Atlanta, GA)	N/A
Human: HEK293T	ATCC	CRL-3216
Mouse: MEF;ARRB1−/−ARRB2−/−	Laboratory of Robert J. Lefkowitz	N/A
Human: HMVEC-L	Lonza	CC-2527
Experimental Models: Organisms/Strains		
Mouse: Sash1+/−: B6.Sash1LacZ/+	Dauphinee et al., 2013	RRID:MGI:5547499
Mouse: eNOS−/−: B6.129P2-Nos3tm1Unc/J	Jackson Laboratory	RRID:IMSR_JAX:002684
Mouse: VEC-Cre:B6;129-Tg(Cdh5-cre)1Spe/J	Jackson Laboratory	RRID:IMSR_JAX:017968

(*Continued on next page*)

Continued

REAGENT or RESOURCE	SOURCE	IDENTIFIER
Mouse: Sash1(fl/fl)	This paper	N/A
Oligonucleotides		
Primer for genotyping, see Table S4	This paper	N/A
Primer for qPCR, see Table S4	This paper	N/A
shRNA targeting ARRB1 mRNA: AAACCCAGGG CTGCCTTGGAAAAG	ThermoFisher	Accessions: NM_004041, NM_020251 Clone ID: TRCN0000005161
shRNA targeting SASH1 mRNA: GCTAATGATG GTCAAAGATTCAAGAGA	Dauphinee et al., 2013	N/A
Control random shRNA sequence: GTTGCTTG CCACGTCCTAGAT	Dauphinee et al., 2013	N/A
SASH1-SAM1 gBlock (sequence on request)	IDT DNA	N/A
Recombinant DNA		
pcDNA3-FlagSASH1	Dauphinee et al., 2013	N/A
pcDNA3-HA-SASH1	Dauphinee et al., 2013	N/A
pEGFPN3-Arrb1	Laboratory of Marc Caron	N/A
pcDNA-Arrb1-HA	This paper	N/A
pMIG-Arrb1(319-418)-HA	This paper	N/A
pMIG-SASH1(SAM1)	This paper	N/A
Software and Algorithms		
Gene Set Enrichment Analysis (GSEA)	PMID: 16199517	N/A
NIH-ImageJ software	https://imagej.nih.gov/nih-image/	N/A
Other		
Microarray analysis service	SickKids Microarray Analysis and Gene Expression Facility	http://www.tcag.ca/facilities/microarray.html
BioRender	https://biorender.com	N/A

CONTACT FOR REAGENT AND RESOURCE SHARING

Further information and requests for reagents may be directed to and will be fulfilled by the Lead Contact, Aly Karsan (akarsan@bcgsc.ca).

EXPERIMENTAL MODEL AND SUBJECT DETAILS

Mice

Sash1 gene-trap mice (C57BL/6 background) (Dauphinee et al., 2013) were maintained as heterozygous (*Sash1*$^{+/-}$) animals and crossed to generate litters of wild-type, heterozygous, and Sash1 null offspring. *Sash1*$^{fl/fl}$ mouse was generated by electroporation into ES cells of a p-loxP-2FRT-PGKneo targeting construct in which *Sash1* exon 3 and 4 are floxed, followed by a stop codon at exon 5. *Sash1*$^{fl/fl}$ mice were crossed with VEC-Cre mice twice to generate VEC-Cre/*Sash1*$^{fl/fl}$ embryos. Drugs were administered to pregnant females by intraperitoneal injection, subcutaneous injection, or oral gavage at specified time points and embryos subsequently harvested. Embryos were genotype using genomic DNA extracted by tail digestion with proteinase K, followed by PCR using specific primers (Table S4). All animal protocols were approved by the Animal Care Committee of the University of British Columbia (Vancouver, British Columbia, Canada).

Cell Lines

Human microvascular endothelial (HMEC) (male) were cultured in MCDB 131 medium. Human embryonic kidney 293T (HEK293T) (sex unknown) and murine embryonic fibroblasts (MEF) (mixed sex) were cultured in Dulbecco's Modified Eagle Medium (DMEM) as previously described (Zhande et al., 2007). For all cell lines, culture medium was supplemented with 10% heat-inactivated fetal bovine serum (FBS), 2mM glutamine, and 100U each of penicillin and streptomycin. For experiments involving LPS stimulation, cells were washed once with serum-free medium and subsequently incubated overnight in medium containing 2% FBS for 12 hours. Cells were stimulated with 100 ng/mL LPS (Sigma-Aldrich, St. Louis, MO) for all indicated times.

METHOD DETAILS

H&E/PAS/IHC

Lung tissues were fixed in 4% paraformaldehyde at 4°C overnight, washed in PBS, then placed in 70% ethanol. Paraffin embedding, sectioning, and hematoxylin and eosin staining was performed at the Centre of Translation and Applied Genomics (CTAG) (BC Cancer Agency – Vancouver Centre, Vancouver, BC). PAS staining was performed using the Periodic Acid Schiff (PAS) kit according to the manufacturer instructions. For immunohistochemical staining, 6 μm paraffin-embedded tissue sections were blocked and incubated with primary antibodies. Detection was performed using the appropriate secondary antibodies and the VectaStain ABC Kit (Vector Laboratories) followed by diaminobenzine staining.

RNA, qRT-PCR, and ddPCR

Lungs were ground in liquid nitrogen with a mortar and pestle on dry ice. Total RNA was extracted using TRIzol reagent (Invitrogen) and cDNA made with Invitrogen SuperScript II reverse transcriptase. qPCR was performed on an Applied Biosystems 7900HT using Power SYBR green (Life Technologies). For digital droplet PCR (ddPCR) experiments, total RNA was extracted using QIAGEN RNeasy Micro kit. ddPCR was performed on BioRad QX200 using EvaGreen supermix (BioRad). Primers are listed in Table S4.

Flow Cytometry

Lung were dissected and cells dissociated in PBS with 2% fetal bovine serum, 550 U/ml collagenase II, IV, 100U/ml DNaseI, and 1% bovine serum albumin (Sigma-Aldrich, St. Louis, MO). Cell suspensions were treated with ammonium chloride (STEMCELL Technologies, Vancouver, Canada), resuspended in PBS-2%FBS with DNaseI and stained with the following antibodies: Alexa Fluor® 488 Anti-Mouse CD326 (Ep-CAM), Anti-Mouse CD45.2 APC-eFluor® 780, Anti-Mouse CD31 (PECAM-1) PerCP-eFluor®710, and APC anti-mouse Podoplanin. Cells were sorted on a BD FACSAria III or BD FACSAria Fusion instrument.

Microarray and Bioinformatics

Endothelial cells were FACS-isolated from the lungs of E18.5 embryos genotyped as *Sash1*$^{-/-}$ (n = 4) and WT (n = 3), and RNA expression analysis using Affymetrix GeneChip® Mouse Gene 2.0 ST Arrays was performed by The Centre for Applied Genomics, The Hospital for Sick Children, Toronto, Canada). Microarray data was normalized using Affymetrix Expression Console (version 1.1). GSEA (version 3.0) was used with recommended settings to compare WT and *Sash1*$^{-/-}$ E18.5 lung endothelial gene expression profiles.

Recombinant Plasmids, Gene Transfer, and RNA interference

pcDNA3-FlagSASH1, pcDNA3-HA-SASH1, and mutant constructs were generated as described (Dauphinee et al., 2013). Rat β-arrestin 1 was cloned from pEGFPN3-Arrb1 (gift from M. Caron, Duke University, Durham, NC) to generate the pcDNA-Arrb1-HA and mutant constructs. SASH1-SAM1 domain construct was generated using a synthetic gBlock (IDT) cloned into a pMSCV-IRES-GFP (MIG) vector. shRNA-mediated knockdown was accomplished via lentiviral-mediated gene transfer and confirmed by immunoblotting. Briefly, lentiviral particles were produced from HEK293T cells co-transfected with 5 μg pLentilox-shSASH1 or pLentilox-shRandom vector, 3 μg pVSVG, 3 μg pREV and 3 μg pRRE per 100 mm dish. For β-arrestin 1, retroviral particles were produced from Phoenix Ampho cells transfected with 10 μg pLKO.1-Puro^{R}-shARRB1 (Thermofisher) or pLKO.1-shSCRAMBLE-Puro^{R} per 100 mm dish. All transfections were carried out using TransIT®-LT1 Transfection Reagent according to the manufacturer's instructions. 48 h and 72 h post-transfection viral supernatants were filtered and used to transduce target cells. RNA Interference Target cells were transduced with shRNAs targeting either human *ARRB1* mRNA (shARRB1), *SASH1* mRNA (shSASH1), or a control random sequence (shRandom) (Dauphinee et al., 2013). See the Key Resource Table for sequences.

Co-Immunoprecipitation, Immunoblotting, and Immunoassay

HEK293T cells were co-transfected with 2-5 μg of each expression plasmid and cell lysates were collected for immunoprecipitation 48 h post-transfection using a modified RIPA buffer (Dauphinee et al., 2013). 1-3 mg of lysates were pre-cleared by incubation with Protein A agarose beads (EMD Millipore Corporation, Billerica, MA) and immunoprecipitated with antibody against SASH1, β-arrestin 1, HA, or control isotype IgG (Sigma-Aldrich, St. Louis, MO) overnight at 4°C, followed by an incubation with TrueBlot® AntiRabbit Ig IP Beads (eBioscience, San Diego, CA) for an additional 3 h at 4°C. Beads were washed four times with RIPA buffer and boiled in Laemmli sample buffer for subsequent immunoblot analysis.

For the immunoprecipitation of Flag-tagged proteins, cell lysates were collected using a Flag-modified RIPA buffer (50 mM Tris-HCl, pH 7.6, 150 mM NaCl, 1 mM EDTA, 1% Triton X-100, plus protease inhibitors) and pre-cleared with Protein G agarose beads. Pre-cleared lysates were added to 50 μL anti-FlagM2-agarose beads or control isotype IgG-agarose and incubated overnight at 4°C. Beads were washed with a Flag-modified wash buffer (50 mM Tris-HCl, pH 7.6, 150 mM NaCl, 0.05% Triton X-100, plus protease inhibitors) and incubated with 0.2 mg/mL FlagM2 peptide for an additional hour at 4°C to elute Flag-tagged proteins. All antibodies are listed in Key Resource Table.

For quantification using capillary immunoassay, protein were separated and detected using Wes Separation Capillary Cartridge 12-230 kDa along with Wes Anti-Rabbit Detection Module. (Simple Western system and Compass Software, ProteinSimple).

Samples were loaded at a 0.2 mg/ml dilution and rabbit antibodies were used against phospho-Akt (1:10), phospho-eNOS (1:10), Akt (1:50), Gapdh (1:50), and β-arrestin1 (1:10).

DAR4M-AM Staining

Pregnant mice were injected with DAR4M-AM (25 μmol/kg intraperitoneally), 1 hour before euthanasia. OCT-embedded sections (10 μm) were fixed in acetone:methanol (1:1) and stained with Hamster anti-CD31 (2H8) primary antibody (1:200), followed by Goat anti-Hamster IgG (H+L) Secondary Antibody, Alexa Fluor 647 conjugated (1:500). Slides were washed overnight and stained with Hoescht 33342. A custom robotic microscope was used to image immunofluorescent staining at 546 nm (DAR4M-AM) and 647 nm (CD31) across entire embryo sections at 0.75 μm/pixel resolution, as previously described (Baker et al., 2008). Images were quantified using customized NIH-ImageJ software (Baker et al., 2008).

In Vitro AE2 Cell Assay

FACS-isolated AE2 cells were plated in Dulbecco's Modified Eagle Medium supplemented with 10% FBS and 1% penicillin-streptomycin/glutamine in a 48-well adherent plate overnight at 37°C. Cells were treated overnight with either 10 μg/ml BAY41-2272 or DMSO (SigmaAldrich, St. Louis, MO), or with 1mM S-Nitroso-N-Acetyl-D,L-Penicillamine (SNAP) or PBS. Cells were lysed, total RNA was extracted and ddPCR was performed as described above.

QUANTIFICATION AND STATISTICAL ANALYSIS

All statistical analyses were calculated using two-tailed Student's t test in GraphPad Prism 7.00 for Windows (GraphPad Software, La Jolla California USA) and considered to be statistically significant at $p < 0.05$. Statistical details can be found in respective figure legend.

DATA AND SOFTWARE AVAILABILITY

Raw data files for the microarray analysis have been deposited in the NCBI Gene Expression Omnibus. The accession number for the microarray data reported in this paper is GEO: GSE123889.